Development of a Knock Prediction Model for Onboard Control in a Spark-Ignited Engine

Seokwon Cho, Chiheon Song, Youngbok Lee, Jihwan Park,
Han Ho Song and Kyoungdoug Min

Seoul National University, 1, Gwanak-ro, Gwanak-gu, Seoul 08826, Republic of Korea

Abstract: As global regulations are becoming increasingly stringent, the development of high-efficiency engines is urgent. A higher compression ratio in an SI (spark-ignited) engine guarantees enhanced thermal efficiency; however, a higher compression ratio also creates knock-prone in-cylinder conditions. Knock generates abnormal heat release, which may cause engine failure; thus, researchers have introduced various strategies to mitigate knock. Advanced ignition timing can provide higher efficiency in high load conditions; however, due to the stochastic behavior of the knock phenomenon, it is difficult to maintain knock-free operations. Therefore, an anticipative knock prediction and control is highly desirable for a better fuel economy.

In this study, experimental tests using a single-cylinder SI engine were demonstrated under various operating conditions, including variations in valve timing. A sophisticated individual cycle analysis was conducted with improvements in the knock onset determination and pressure filtering method. By introducing various methods, such as modeling the RGF (residual gas fraction), heat loss and burn duration, in-cylinder pressure could be predicted with high accuracy. Based on the predicted pressure, fast knock prediction was achieved using the 0D (zero-dimensional) ignition delay correlation and the given knock criterion.

As a result, the established model could predict the knock propensity in real-time, which allows high-fidelity control of ignition timing, leading to an enhanced thermal efficiency.

1. Introduction

One of the greatest issues in the history of spark-ignited engine development is increasing the compression ratio because the compression ratio has a direct relationship with efficiency [1]. Recently, as global regulations for emission and fuel efficiency have become increasingly stringent, companies with the capability of mass production and a substantial number of researchers have been trying to develop engines with higher efficiency.

Although a higher compression ratio enables higher engine efficiency, the compression ratio should be limited because of the occurrence of knock. Knock is an abnormal combustion in which the air-fuel mixture is autoignited in an unburned gas region under high pressure and temperature conditions [1-3]. Knock is accompanied by a troublesome noise and transmits vibration to the engine. Moreover, engine failure can occur if knock occurs continuously.

Advancing ignition timing is one of the most promising methods to secure high efficiency [4]; however, advanced ignition timing generally induces knock-prone conditions due to high pressure and temperature conditions in the unburned gas region. Therefore, knock must be mitigated when advancing ignition timing.

Because the compression ratio is not easily controlled in a specific engine design, knock behavior during the engine operation is practically suppressed by retarding the ignition timing. Traditional engines use passive control for knock suppression. The knock sensor mounted on the engine block detects the vibration that occurs when in-cylinder knock occurs. Then, by filtering the signal, the ECU (engine control unit) considerably retards the ignition timing to mitigate knock.

This type of knock control has several limitations, as the control is involved after knock occurs. Unnecessary vibration and noise are delivered to the driver when knock occurs, and the engine is also damaged [3]. Passengers would feel inconvenienced by retarding the ignition timing, which provokes a sudden decrease in engine torque and a corresponding deceleration of the vehicle. Additionally, the unit production price increases by mounting an additional sensor on the engine. Furthermore, there is a heat loss by running an engine with retarded ignition timing instead of in optimal conditions.

To overcome these limitations, knock should be actively controlled. Active control of knock involves predicting the occurrence of knock, which allows the engine to be run without knocking by selecting moderate operating parameters in advance. By introducing active knock control, heat loss can be reduced by a moderate ignition timing, and engine damage can also be minimized. In addition, as the calculation required for knock prediction can be conducted using the ECU, a knock sensor is no longer necessary. The removal of the sensor from the structure decreases the unit production price of the engine.

Knock can be predicted by calculating the ignition delay. The ignition delay at a certain state can be estimated in some ways, such as using a 0D empirical

correlation [5-7] or solving a detailed chemical mechanism. For real-time control, a 0D empirical correlation must be used due to its fast calculation speed. However, conventional knock prediction models based on a 0D empirical ignition delay correlation rely exclusively on in-cylinder pressure measurements. However, because in-cylinder pressure transducers are very expensive for mass-production engines, pressure prediction-based knock control is required. Based on the prediction of pressure, the onset of knock can be calculated from the Livengood-Wu integral method [8]. Moreover, a knock criterion must be defined to create a knock model because the Livengood-Wu integral method does not provide the knock propensity; the Livengood-Wu integral method gives only the timing of autoignition.

This study mainly consists of five sections, including this introduction. The next section describes the configurations for the engine experiment. The following section presents the detailed methodologies for establishing the models. The next section presents a validation result. The final section presents the conclusions of the study.

2. Experimental Setup and Conditions

2.1 Engine setup and specifications

Experimental tests were conducted using a single-cylinder N/A (naturally aspirated) PFI (port fuel injection) engine. The engine had a displacement volume of 0.5 L. The bore and stroke were 81 mm and 97 mm, respectively, and the compression ratio was 12. A schematic diagram of the experimental engine system and the details of the system are shown in figure 1 and table 1, respectively.

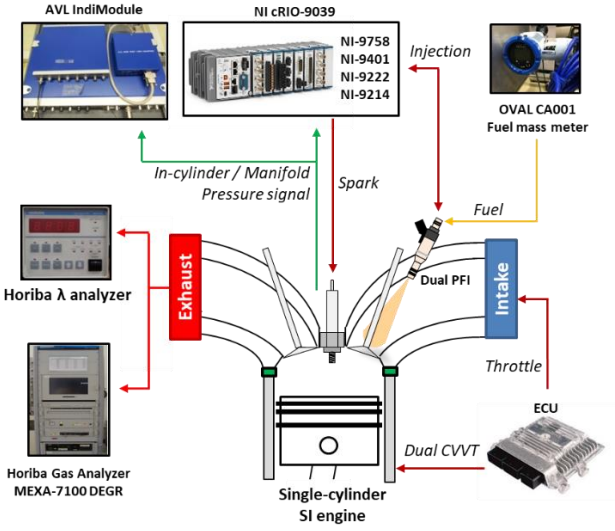

Figure 1: Schematic diagram of the engine test

Dual CVVT (continuous variable valve timing) modules for both intake and exhaust were controlled with an ECU using ETAS INCA software. The intake valve timing could be advanced within a 50 CA (crank angle) range from its parking position, whereas the exhaust valve timing could be retarded within a 40 CA range. A rotary encoder with 3600 ticks was utilized for engine control and data acquisition. Thanks to the 0.1 CA resolution of the encoder, the engine control was highly precise and the data acquisition had high resolution for knock analysis.

AVL Indimodule and Indicom 2.0 software were used to log the pressure data. In-cylinder pressure was measured using a Kistler 6056A piezoelectric in-cylinder pressure transducer, and the sensor was flush-mounted in the cylinder head near the spark plug. The acquired raw pressure signal was amplified by an AVL IFEM amplifier, and the intake manifold pressure was measured using a Kistler 4045A5 sensor. The signal was amplified using a Kistler 4603 amplifier.

A Horiba MEXA-7100 DEGR gas analyzer was used for emissions monitoring and for controlling the air-fuel ratio during the experiment; a Horiba MEXA-110λ analyzer was also used for monitoring. The fuel flow rate was monitored with an OVAL CA001 Coriolis fuel flowmeter.

Table 1: Experimental engine specifications

Engine type	Single-cylinder N/A dual CVVT
Displacement	499.8 cc
Bore	81 mm
Stroke	97 mm
Compression ratio	12 : 1
EVO / EVC	bBDC 68° / aTDC 1°
IVO / IVC	aTDC 10° / aBDC 67°
Number of valves	4
Max valve lift	10 mm (both)
Injection system	Dual PFI, 6 bar

2.2 Experimental conditions

The experimental conditions are shown in table 2. Engine test was conducted under wide operating conditions to achieve higher model validity. The engine speed was varied from 1000 to 2000 rpm. During the operation, the air-fuel ratio was maintained at the stoichiometric condition, which allowed the utilization of the exhaust catalyst. The engine load was varied up to 9.5 bar of nIMEP (net indicated mean effective pressure) by changing the intake pressure and ignition timing; thus, the knock propensity

exhibited by the parametric variation from 0 to over 50%. One of the most important aims of this study was to ensure validity under various valve timing conditions, which largely affect the residual gas fraction and ignition delay; hence, the valve overlap was changed using CVVT modules from a negative valve overlap of 3 CA to a positive valve overlap of 47 CA. The ambient, oil and coolant temperatures were maintained at the same levels shown in table 2 by using the controllers. A conventional gasoline fuel with a LHV (low heating value) of 42.825 MJ/kg was used as an engine fuel. The octane number of the fuel was 91.5, and detailed specifications of the fuel and the testing methods are listed in table 3.

Table 2: Test conditions

Engine speed	1000 – 2000 rpm
Ignition timing	28 CA bTDC – 4 CA aTDC
Maximum engine load	9.5 bar
Intake pressure	0.6 – 0.9 bar
Ambient temperature	25 ± 1 °C
Oil/Coolant temperature	85 ± 2 °C

Table 3: Test fuel properties

Conventional gasoline	Value	Test Method
H/C ratio	2.064	ASTM D 5291
Density [kg/m^3] @ 15 °C	724.5	ASTM D 1298
Research Octane Number	91.5	ASTM D 2699
LHV [MJ/kg]	42.825	ASTM D 240-14
Oxygen [mass %]	1.53	ASTM D 4815
Methanol [mass %]	< 0.05	ASTM D 4815

2.3 Knock detection

Knock detection during the engine experiment was facilitated by using an in-cylinder pressure transducer; this method is widely used because it is very versatile and reliable. To capture the pressure oscillation generated by the autoignition of end gas, this study adopted a high-pass filtering strategy with the nine-point median filter expressed in equations 1 and 2. As shown in equation 3, a cycle was judged as a knocking cycle if the maximum amplitude of the filtered signal exceeded 0.5 bar, which is the MAPO (maximum amplitude pressure oscillation) TVE (threshold value exceeded) method.

$$P_{med,n} = \frac{(P_{n-4}+P_{n-3}+\cdots+P_{n+3}+P_{n+4})}{9} \quad [1]$$

$$P_{filt} = P - P_{med} \quad [2]$$

$$|P_{filt}| > 0.5\ bar \quad [3]$$

Because knocking behavior is highly stochastic, a statistical approach is essential to the determination of the knocking propensity. In this study, the knock incidence method [4, 9-11] shown in expression 4 was applied while the total cycle number was greater than or equal to a thousand during the consecutive steady-state operation [10].

$$MAPO\ Incidence = \frac{N_{knock}}{N_{total}} \times 100\ [\%] \quad [4]$$

2.4 Knock onset determination using supervised deep learning

This chapter describes an attempt to find the actual position of knock onset. The knock onset position in a knock cycle should be determined to establish a high-fidelity knock prediction model. The TVE method has been widely used for knock onset determination. The TVE method determines the knock onset as the timing at which the value of the filtered pressure exceeds a specific threshold value. However, this method tends to determine a knock onset position that is later than the real knock onset position.

Various algorithms have been developed for reducing the error between the estimated knock onset and actual position. Kim [12] assumed a calculation window in each pressure data cycle and set a threshold value for each cycle using the mean and standard deviation of the pressure signal values of the calculation window. Shahlari [13] assumed a linearly extrapolated line and found the position at which the given data and the extrapolated data started to deviate from one another. Both methods exhibited lower accuracy under weak knock conditions, and these methods created a possibility of cycle loss because they were developed and validated under heavy knock conditions.

Heavy knock conditions generally represented over 50% of knock incidence during the steady-state engine experiment, so it was already beyond the purpose of development of the knock prediction model in this study. As this study focused on the substitution of a knock sensor with a virtual knock sensor, an advanced knock determination method including weak knock conditions was necessary. Therefore, a determination algorithm from the authors'

previous study [10] using supervised deep learning was applied.

The result of the improved determination method is shown in figure 2. The figure shows a low and reasonable RMSE (root mean squared error) value between the actual knock onset (achieved by mouse-clicking method) and estimated knock onset. In addition, there was no cycle loss even in the weak knock operation. Based on the achieved high-accuracy knock onset data, a 0D-based empirical ignition delay model could be created, which is presented later in this paper.

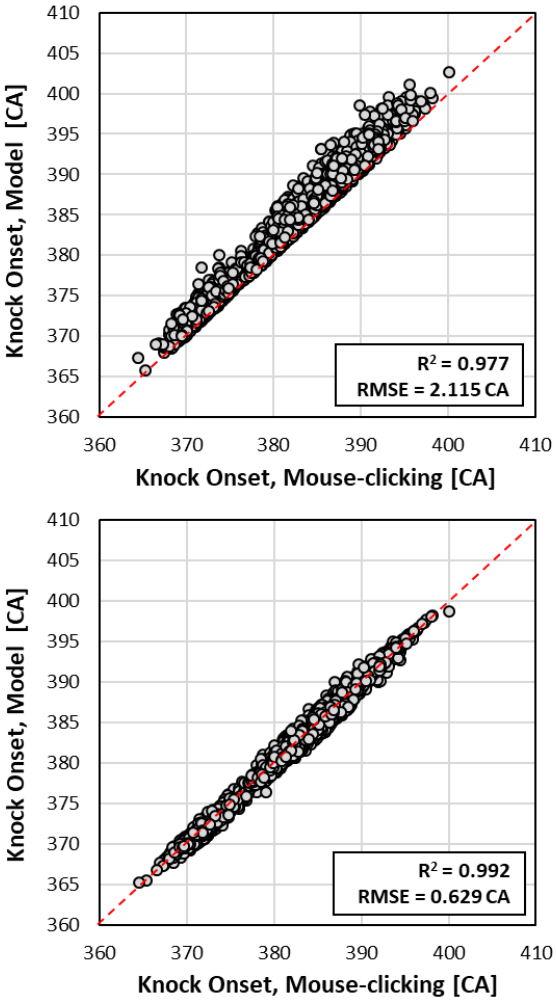

Figure 2: Knock onset determination methods: (a) the conventional TVE method and (b) the improved method using supervised deep learning [10]

3. Detailed Modeling Process

As previously described, the final objective of this process is to predict the knock propensity without using a knock sensor. Additionally, because in-cylinder pressure sensors cannot be used in mass-production engines due to their high cost, only the intake MAP (manifold absolute pressure) sensor has to be used at the beginning of the entire process. This chapter describes the overall procedure in this paper, from the intake pressure value achieved by the MAP sensor until the knock prediction.

Knock prediction in this study was established using estimated in-cylinder pressure. For real-time-based knock prediction and control, the 0D approach was inevitably essential due to the finite time scale of engine control. As the in-cylinder pressure is a good indicator for the calculation of the in-cylinder temperature, the in-cylinder pressure can be predicted by using a simple 0D single-zone based approach, and the in-cylinder condition can be determined from the predicted pressure.

In this study, the process consists of four steps. In the first stage, the gas state at IVC (intake valve closing) was estimated. For a closed system analysis and prediction, the initial conditions of in-cylinder gas, such as the pressure, temperature and composition, had to be identified. Second, pressure modeling during compression until ignition timing was achieved using the estimated state from the first stage. Third, heat release was modeled to estimate the in-cylinder pressure after the ignition timing until EVO (exhaust valve opening). Last, a knock prediction model based on a 0D ignition delay correlation was applied in addition to a statistical approach. Figure 3 shows the overall process for easier interpretation, and the following chapters describe the detailed methodologies for each process of pressure modeling and knock prediction.

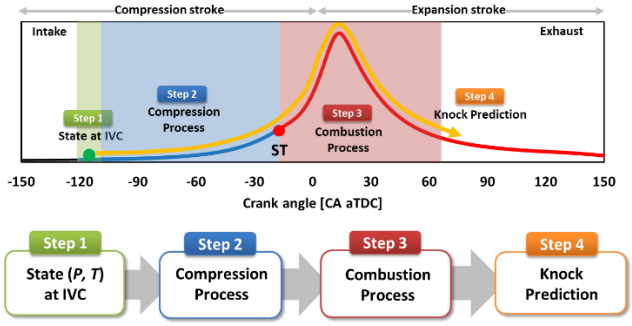

Figure 3: Overall modeling process

3.1 Estimation of the IVC condition

To predict the knock occurrence, the pressure trace should be properly predicted. An imprecise prediction of the initial gas state at IVC timing leads to critical errors in the whole estimation process; a reliable estimation is required because a small error creates a large difference after the compression and combustion processes.

For a correct estimation of the IVC condition, two main things should be considered: the pressure and the gas composition. If the pressure and gas

composition were properly estimated, the temperature can be simply calculated as follows:

$$T_{IVC} = \frac{P_{IVC}V_{IVC}}{(n_{fuel}+n_{air}+n_{residual})R} \quad [5]$$

The in-cylinder pressure at IVC timing can be achieved based on the intake pressure value obtained by the MAP sensor installed on the intake manifold, and the volume can be determined from a simple calculation of the engine geometry. In addition, the mixture properties can be determined based on the ECU input fuel mass with an estimation of the RGF.

3.1.1 In-cylinder pressure at IVC timing

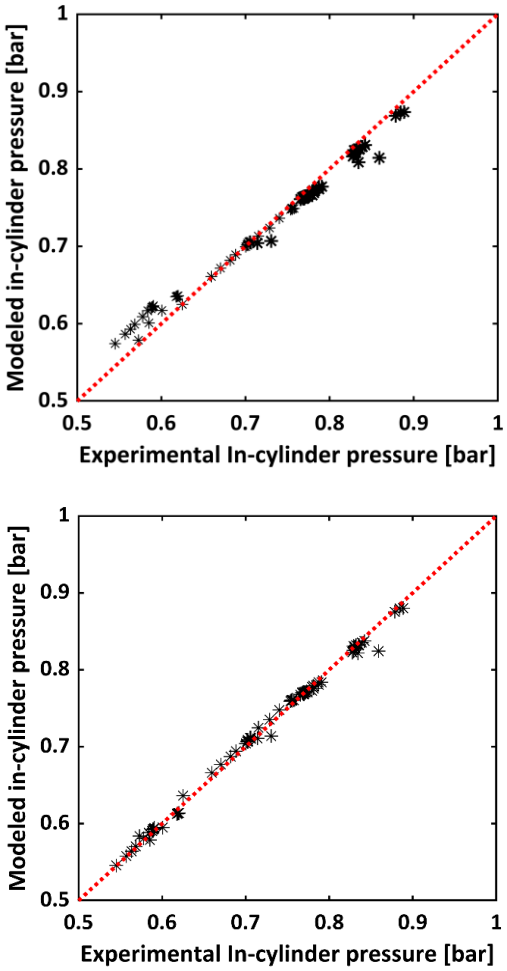

Figure 4: Estimation of the in-cylinder pressure at IVC timing using intake pressure: (a) Eriksson's method [14] and (b) the improved method

This chapter describes an attempt to obtain the estimated in-cylinder pressure value at IVC timing from the intake pressure. An early attempt was made by Eriksson et al. [14], and the empirical correlation shown in equation 6 was suggested considering the engine speed.

$$P_{IVC} = P_{MAN} + C_1 + C_2 Speed \quad [6]$$

The result of Eriksson's existing model is shown in figure 4(a). These results showed a lower correlation in valve overlap cases because the empirical model does not involve the effect of RGF variation. Thus, in this study, to indirectly incorporate the effect of RGF variation, the valve overlap effect was also considered using the valve overlap factor (OF) introduced by Fox et al. [15] for RGF estimation. The new suggested expressions are as follows:

$$P_{IVC} = P_{MAN} + C_1 + C_2 Speed + C_3 OF \quad [7]$$

$$OF = \frac{D_{In}\int_{\theta_{IVO}}^{L_{In}=L_{Ex}} L_{In}d\theta + D_{Ex}\int_{L_{In}=L_{Ex}}^{\theta_{EVC}} L_{Ex}d\theta}{V_d} \quad [8]$$

Figure 4(b) shows the improved estimation result of in-cylinder pressure at IVC timing. This result showed a reasonable correlation for the initial guess of the closed system analysis and estimation. Therefore, after this process, the pressure and volume were achieved, so the RGF is the last factor that must be determined to properly estimate the initial gas condition.

3.1.2 Residual gas fraction

As previously described, estimation of the gas composition is critical because it affects not only the calculation of the gas temperature at IVC timing but also other processes such as compression and combustion.

Several 0D models for estimating residual gas fraction have been suggested. Fox et al. introduced a model considering the trapped gas mass in the cylinder after the combustion process and backflow gas mass during the valve overlap period. The overlap factor shown in equation 8 was introduced in this model to quantify the valve overlap period.

The total residual gas fraction can be expressed by summing the trapped mass term and backflow term. These expressions are as follows:

$$RGF = RGF_{Backflow} + RGF_{IVC} \quad [9]$$

$$RGF_{Backflow} = C_1 \left(\frac{P_e}{P_i}\right)^{\frac{\gamma+1}{2\gamma}} \frac{OF}{RPM}\sqrt{\frac{P_e - P_i}{\rho_a}} \quad [10]$$

$$RGF_{IVC} = C_2 \left(\frac{P_e}{P_i}\right)^{\frac{1}{\gamma}} / r_c \quad [11]$$

Kale et al. [16] revised Fox's model by considering various valve timing and additional valve overlap factors, which can be separated into two types. One of the considerations was the position of TDC during valve overlap, and the other was the timing at which valve curtain areas of the intake and exhaust valves become the same. A detailed description of the model is avoided in this paper because it is very well described in their study.

Although Kale's model showed a reasonable agreement with the test data in this study (R^2 = 0.763), an improvement was still necessary for the preciseness, particularly for high volumetric efficiency conditions. A revised model [10] based on Kale's model was used in this study, and a further consideration of volumetric efficiency showed a better performance (R^2 = 0.883). The attempt was made utilizing a 1D (one-dimensional) simulation (GT-power) and DoE (design of experiments) process. Figure 5 shows the results of the improved 0D RGF model.

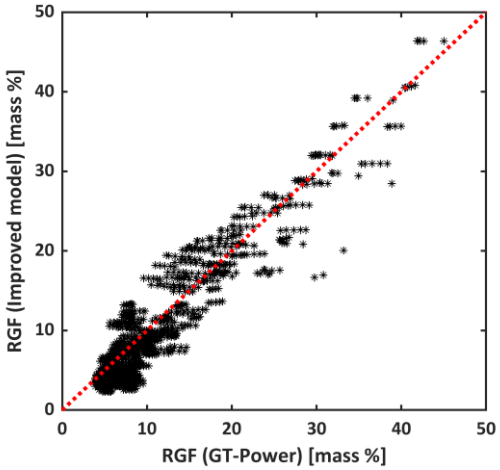

Figure 5: Improved 0D RGF model [10]

3.2 Compression process

As the initial condition of the gas mixture was estimated in the previous step, the in-cylinder pressure during the compression was modeled until the ignition timing. The ignition timing for a certain operating condition is normally determined by MAP-based calculations in the ECU of a mass-production engine. In this process, the pressure was predicted until predetermined ignition timing; however, if it is adapted for onboard control in the future, an efficient method for feedback control is still required.

During the compression stroke, the in-cylinder mixture is compressed by the upward movement of the piston. This process is generally considered an adiabatic compression. However, there is still heat transfer between the in-cylinder gas and the cylinder walls. In addition, the specific heat ratio during compression varies rapidly as the gas temperature increases; the specific heat ratio is generally known as a function of temperature and gas composition. Figure 6 shows an example of an error in the predicted pressure value under the adiabatic process assumption. Even if a correct value of the specific heat ratio at IVC was used, the error can gradually increase until the prediction reaches the ignition timing because of the two reasons mentioned above. Therefore, compensation for this error between the specific heat ratio and polytropic index was still required for the accurate estimation of the in-cylinder pressure until ignition timing [17].

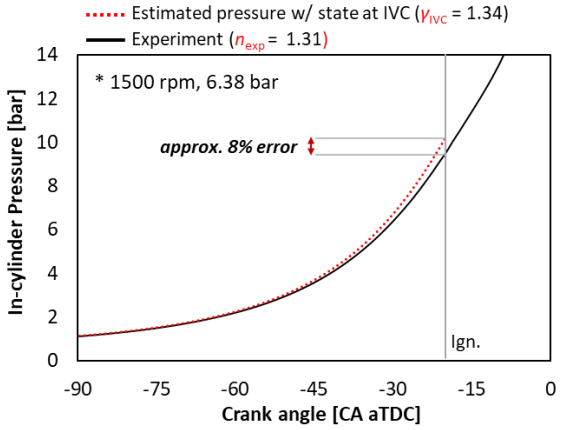

Figure 6: Necessity of polytropic index correlation

To compensate for the error and to simply assume the compression as a polytropic process for fast calculations, this study suggests a new method that uses a polytropic index during the compression period. As the initial gas state of the closed system was achieved in the previous step, the index could be achieved with a specific heat ratio at IVC, the effective volumetric ratio of IGN (ignition), the IVC timings, and the engine speed, which reflects the amount of heat loss.

$$n_{model,comp} = f(\gamma_{IVC},\ V_{IVC}/V_{IGN},\ Speed) \quad [12]$$

$$n_{exp} = log\left(\frac{P_2}{P_1}\right) / log\left(\frac{V_1}{V_2}\right) \quad [13]$$

$$P_{model} = P_{IVC}\left(\frac{V_{IGN}}{V_{IVC}}\right)^{n_{model,comp}} \quad [14]$$

Figure 7 shows the results of the compression process. The x-axis indicates the in-cylinder pressure at ignition timing from the experimental results, and the y-axis indicates the modeled in-cylinder pressure at ignition timing. For all experimental cases, an excellent correlation was achieved: the R^2 value was 0.9986 and the RMSE was 0.078 bar.

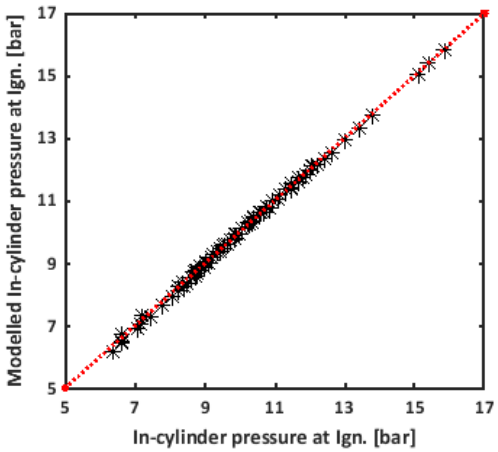

Figure 7: Comparison of in-cylinder pressures between model and experiment at ignition timing

3.3 Combustion process

After the ignition timing, the combustion begins from the location of the spark plug. Combustion extracts the chemical energy from the fuel to increase the pressure and temperature in the chamber; this is the main power source of an internal combustion engine. If the heat released by chemical reactions is appropriately estimated, in-cylinder pressure and temperature can be correctly predicted by considering energy conservation with a few assumptions. There have been several studies to describe the heat release of combustion in various operating ranges [18-20]. In this study, an attempt using a representative heat release curve was made for the pressure estimation during the combustion period.

3.3.1 Representative heat release curve

The heat release rate changes significantly when the operating conditions are changed, and the heat release rate also varies during the steady-state operation due to cyclic variations. Each condition has its own ignition timing, burn duration and total heat amount; hence, every curve exhibits a different shape.

In this study, for fast calculations, an approach using a representative curve was applied [21, 22]. Each curve was normalized in the horizontal direction by its burn duration and normalized in the vertical direction by its total heat amount. Figure 8 shows the results of this normalization process, and it is shown that it can be represented by one curve. For burn duration, the value of CA0 – CA90 was used because it is difficult to define the EOC (end of combustion) and knock normally occurs before CA90.

$$\frac{Q_{net}(\theta)}{Q_{fuel} - Q_{loss}} = 1 - exp\left[-a\left(\frac{\theta-\theta_{ST}}{\Delta\theta_{0-90}}\right)^{m+1}\right] \quad [15]$$

$$Q_{norm}(\theta) = 1 - exp[-a \cdot (\theta_{norm})^{m+1}] \quad [16]$$

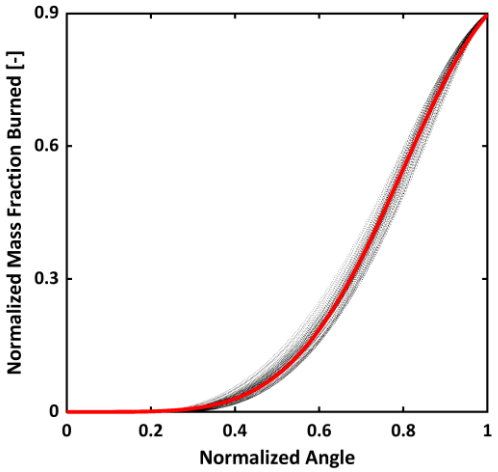

Figure 8: A representative MFB curve based on normalizing the experimental data

Equations 15 and 16 are Wiebe functions of the heat release and normalized heat release for simplification, respectively. To predict the in-cylinder pressure during combustion, total heat loss and burn duration are still required to determine the actual heat release curve from the normalized mass burn fraction curve [21]. Therefore, the modeling of both parts was conducted.

3.3.2 Modeling heat transfer and burn duration

The total heat transfer loss value is difficult to estimate because there is an uncertainty in the EOC timing for the experimental data even though there are various heat transfer models, such as Woschni [23] and Hohenberg [24] models. In this study, regardless of the precision of the heat transfer value, the reconstruction of the heat release curve was a greater focus. Thus, the estimation of the heat transfer loss during the combustion analysis was the target for this modeling. The combustion analysis used in this study has also been interpreted in previous studies [10, 25]. Figure 9(a) shows the results of heat loss modeling, which had a satisfactory correlation (R^2 = 0.956).

$$Q_{loss} = f(Q_{fuel}, Speed, \theta_{ign}) \quad [17]$$

In addition, as the burn duration also varies under different operating conditions, a burn duration model was required to utilize the representative (normalized) heat release curve. For burn duration, this study used a model previously suggested by Bonatesta et al. [26], as shown in equation 18, and the model showed good agreement with the experimental results. In this study, the coefficients were newly calibrated to match the results of combustion analyses, and the burn duration

was modified as CA10 – CA90 as previously described.

$$\Delta\theta_{0-90} = f(m_{fuel}, Speed, \theta_{ST}) \quad [18]$$

Figure 9(b) is the result of burn duration modeling, and the result also showed a nice correlation (R^2 = 0.833) for the overall engine operating condition.

3.3.3 Prediction of the in-cylinder pressure during the combustion period

Equation 19 shows the equation used to construct the in-cylinder pressure based on the estimated heat release curve [21]. For the combustion period, the specific heat ratio was simply set as a constant (1.3) for fast calculations because it is still acceptable if the predicted in-cylinder pressure is well matched to the original one. However, in some WOT (wide open throttle) conditions, this approach resulted in a lower accuracy due to the low heat oxidation phenomenon. Thus, further investigation is still required.

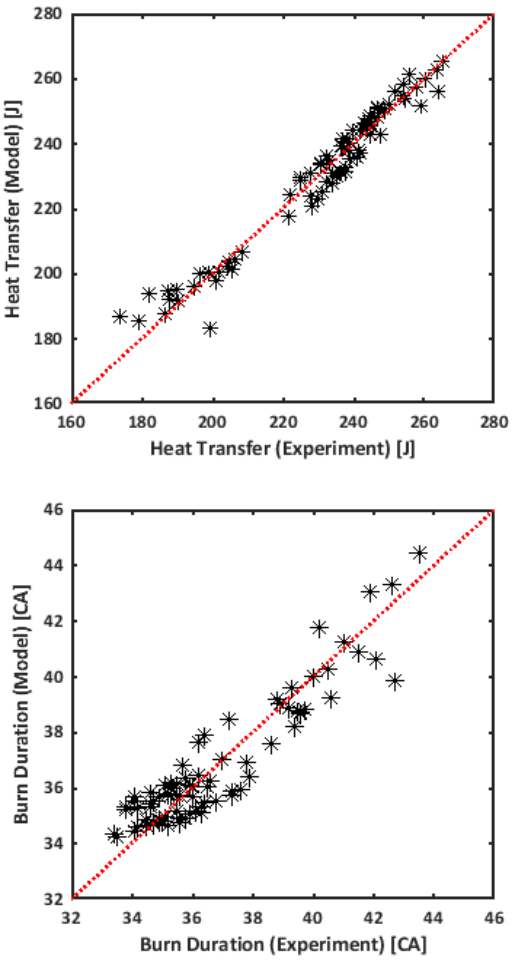

Figure 9: Modeling results: (a) heat loss and (b) burn duration

$$P_n = \frac{\frac{dQ_{net}}{d\theta} - \frac{\gamma}{\gamma-1}P_{n-1}\frac{dV}{d\theta}}{\frac{1}{\gamma-1}V_{n-1}\frac{1}{\Delta\theta}} + P_{n-1} \quad [19]$$

Figure 10 shows several examples of the comparison of the predicted in-cylinder pressure (indicated with the red line) and the actual in-cylinder pressure from the experiment (indicated with the black line). The results show that the in-cylinder pressure prediction was well achieved.

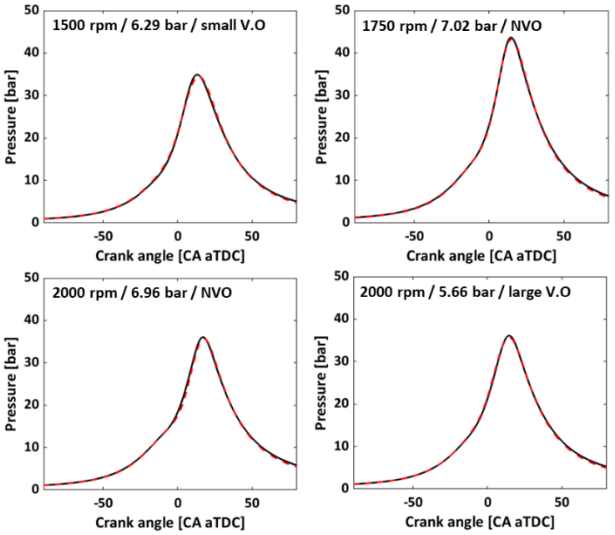

Figure 10: Results of in-cylinder pressure prediction

3.4 Knock modeling

3.4.1 Calibration of the 0D ignition delay

$$\tau = C_1 \left(\frac{P}{T}\right)^{-C_2} exp\left(\frac{C_3}{T}\right) \quad [19]$$

$$\frac{(x)}{(x_c)} = \int_{\theta_{IVC}}^{\theta} \frac{1}{\tau} dt = 1 \quad [20]$$

Knock behavior was predicted based on the 0D ignition delay correlation in this study. There have been numerous studies on the empirical correlation of 0D ignition delay based on experimental results [5-7, 10]. As a first step and for fast calculations, the simple model shown in equation 19 was used with the Livengood-Wu correlation, which is shown in equation 20.

The coefficients were calibrated using a genetic algorithm, and the experimental knock onset data were extracted using the described methodology in section 2.4. Figure 11 shows the validity of the established model. The x-axis indicates the knock onset from the experimental data, and the y-axis indicates the model-predicted knock onset. For the overall testing points, an RMSE of 0.99° CA was achieved.

The knock prediction model in this study was established within limited operating conditions. In addition, as previously described, the 0D ignition delay correlation shows a less strong performance under full load conditions, which is mainly due to low heat oxidation. Thus, to incorporate other effects such as dilution, EGR (exhaust gas recirculation) and phenomena caused by extremely high load conditions, further study is still required.

Furthermore, the established model predicts the knock onset using only single-cycle predicted pressure data. As the final goal is to predict the knock propensity in certain operating conditions, an investigation of the criterion for determining knock propensity or incidence is essential. Otherwise, the proposed approach cannot replace conventional knock sensors.

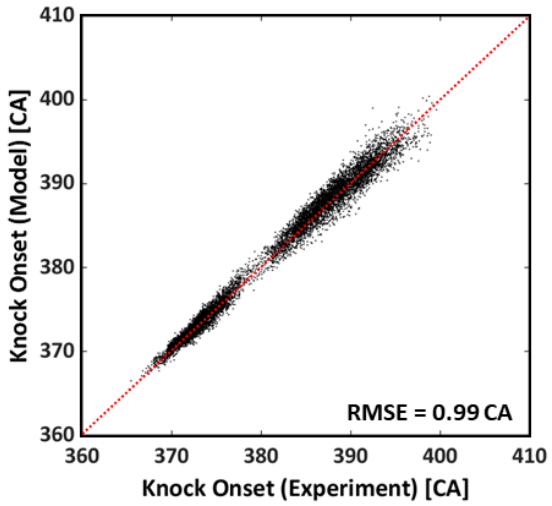

Figure 11: Knock prediction model

3.4.2 Knock criterion

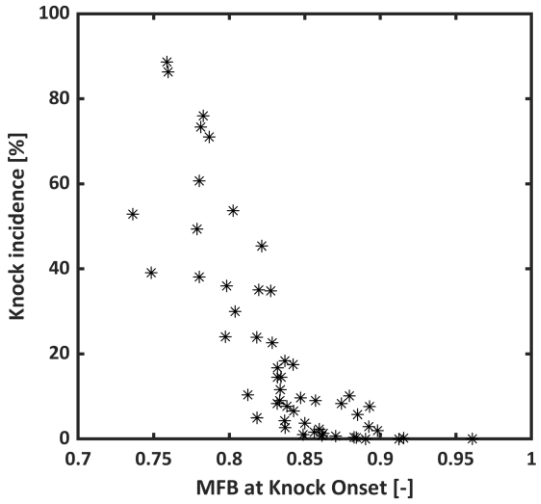

Figure 12: Knock incidence and MFB at knock onset

Figure 12 depicts the relationship between knock incidence and MFB (mass fraction burned) at knock onset. From the figure, it is clearly shown that knock behavior is drastically suppressed when the unburned mass fraction is less than 10%, which means that the energy of the unburned mixture is insufficient to develop to a strong autoignition. In this study, by parametric analysis, the MFB85 (85% mass fraction burned) timing was determined as a criterion. Figure 13 shows the concept of the MFB85 criterion. Based on the predicted in-cylinder pressure, the ignition delay can be calculated using the established ignition delay correlation. Afterward, the timing of knock occurrence (knock onset) can be predicted, and if it is located prior to the MFB85 timing, it is judged as a knocking cycle.
This criterion can be varied when the standard for knock is changed. However, in this study, a satisfactory separation of knocking conditions and nonknocking conditions was shown.

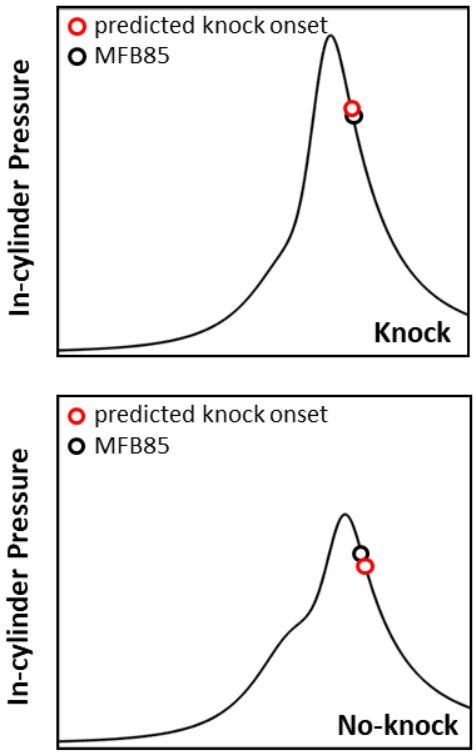

Figure 13: Concept of the MFB85 knock criterion

4. Validation

In the previous sections, a knock prediction model was developed based on estimated in-cylinder pressure. Finally, the knock model was completed by applying a criterion to anticipate the knock propensity. The developed knock model was validated under experimental conditions. Figure 14 shows the knock incidence anticipated by the model against the actual knock incidence value during the experiment. It is

easily found that the developed model predicts knocking behavior with high accuracy.

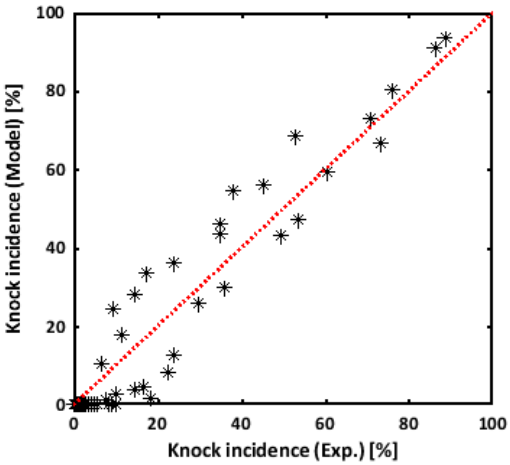

Figure 14: Validity of the knock prediction model

5. Conclusions

In this study, a knock prediction model was developed to replace the conventional knock sensor. To ensure the validity of the model, several attempts were made in this study:

1. As the model had to predict the knock occurrence and its propensity prior to knock occurrence, in-cylinder pressure prediction was required.
2. For in-cylinder pressure prediction, a method was proposed to estimate the initial conditions of a closed system. This method included in-cylinder pressure calculations based on the MAP sensor and an improved 0D RGF model.
3. The compression period was satisfactorily modeled using the adiabatic process assumption and a compensated polytropic index method.
4. The combustion process was modeled by introducing a representative mass fraction burned curve, modeling the heat loss and burn duration and reconstructing the in-cylinder pressure.
5. A knock prediction model using the 0D ignition delay correlation and the Livengood-Wu integral method was established. Based on this model, a criterion (MFB85) was suggested to anticipate the knock propensity.
6. The developed knock prediction model showed a remarkable correlation with the experimental data, which promises future knock control that increases efficiency by preventing unnecessary retardation of ignition timing.

6. Acknowledgments

The authors would like to express deep gratitude to Dr. Kyoung-pyo Ha and senior researchers Backsik Kim and Ingee Suh of the Hyundai Motor Company for their unconditional support. This work was also supported by the BK21 Plus program through the National Research Foundation (NRF) funded by the Ministry of Education, Republic of Korea.

7. References

1. Heywood, J. B. *Internal Combustion Engine Fundamentals.* NewYork: McGraw-Hill, 1988.
2. Zhen, X., Wang, Y., Xu, S., Zhu, Y. et al. "The engine knock analysis–an overview." *Applied Energy* 92:628-36, 2012, doi:10.1016/j.apenergy.2011.11.079.
3. Wang, Z., Liu, H., and Reitz, R. D., "Knocking combustion in spark-ignition engines." *Progress in Energy and Combustion Science* 61:78-112, 2017, doi:10.1016/j.pecs.2017.03.004.
4. Cho, S., Song, C., Oh, S., Min, K. et al. "An Experimental Study on the Knock Mitigation Effect of Coolant and Thermal Boundary Temperatures in Spark Ignited Engines." SAE Technical Paper 2018-01-0213, SAE International, 2018, doi:10.4271/2018-01-0213.
5. Douaud, A. and Eyzat, P. "Four-Octane-Number Method for Predicting the Anti-Knock Behavior of Fuels and Engines." SAE Technical Paper 780080, 1978, doi:10.4271/780080.
6. Chen, L., Li, T., Yin, T., and Zheng, B., "A predictive model for knock onset in spark-ignition engines with cooled EGR." *Energy Conversion and Management* 87:946-55, 2014, doi:10.1016/j.enconman.2014.08.002.
7. McKenzie, J. and Cheng, W. K. "Ignition Delay Correlation for Engine Operating with Lean and with Rich Fuel-Air Mixtures." SAE Technical Paper 2016-01-0699, 2016, doi:10.4271/2016-01-0699.
8. Livengood, J. and Wu, P. "Correlation of autoignition phenomena in internal combustion engines and rapid compression machines." Paper presented at the Symposium (international) on combustion, 1955. doi:10.1016/S0082-0784(55)80047-1.
9. Cho, S., Oh, S., Song, C., Shin, W. et al. "Effects of Bore-to-Stroke Ratio on the Efficiency and Knock Characteristics in a Single-Cylinder GDI Engine." SAE Technical Paper, SAE International, 2019, doi:10.4271/2019-01-1138.
10. Cho, S., Park, J., Song, C., Oh, S. et al. "Prediction Modeling and Analysis of Knocking Combustion using an Improved 0D

RGF Model and Supervised Deep Learning." *Energies* 12(5):844, 2019, doi:10.3390/en12050844.
11. Oh, S., Cho, S., Seol, E., Song, C. et al. "An Experimental Study on the Effect of Stroke-to-Bore Ratio of Atkinson DISI Engines with Variable Valve Timing." *SAE Int. J. Engines* 11(6):1183-93, 2018, doi:10.4271/2018-01-1419.
12. Kim, K. S. "Study of engine knock using a Monte Carlo method." Ph.D Dissertation, The University of Wisconsin-Madison, 2015.
13. Shahlari, A. J. and Ghandhi, J. "Pressure-Based Knock Measurement Issues." SAE Technical Paper 2017-01-0668, 2017, doi:10.4271/2017-01-0668.
14. Eriksson, L. and Andersson, I. "An Analytic Model for Cylinder Pressure in a Four Stroke SI Engine." SAE International, 2002, doi:10.4271/2002-01-0371.
15. Fox, J. W., Cheng, W. K., and Heywood, J. B. "A Model for Predicting Residual Gas Fraction in Spark-Ignition Engines." SAE International, 1993, doi:10.4271/931025.
16. Kale, V., Yeliana, Y., Worm, J., and Naber, J. "Development of an Improved Residuals Estimation Model for Dual Independent Cam Phasing Spark-Ignition Engines." SAE International, 2013, doi:10.4271/2013-01-0312.
17. Lee, Y. and Min, K., "Estimation of the Polytropic Index for In-cylinder Pressure Prediction in Engines." *Applied Thermal Engineering* 2019/04/25/ 2019, doi:10.1016/j.applthermaleng.2019.04.113.
18. Ghojel, J. I., "Review of the development and applications of the Wiebe function: A tribute to the contribution of Ivan Wiebe to engine research." 11(4):297-312, 2010, doi:10.1243/14680874jer06510.
19. Finesso, R., Spessa, E., Yang, Y., Alfieri, V. et al. "HRR and MFB50 Estimation in a Euro 6 Diesel Engine by Means of Control-Oriented Predictive Models." *SAE Int. J. Engines* 8(3):1055-68, 2015, doi:10.4271/2015-01-0879.
20. Yasar, H., Soyhan, H. S., Walmsley, H., Head, B. et al. "Double-Wiebe function: An approach for single-zone HCCI engine modeling." *Applied Thermal Engineering* 28(11):1284-90, 2008/08/01/ 2008, doi:10.1016/j.applthermaleng.2007.10.014.
21. Lee, Y., Lee, S., Han, K., and Min, K. "Prediction of In-Cylinder Pressure for Light-Duty Diesel Engines." SAE International, 2019, doi:10.4271/2019-01-0943.
22. Lee, S. "Modeling of a real-time virtual pressure and NOx sensor for light-duty Diesel engines." Ph.D. Dissertation, Seoul National University, 2017.
23. Woschni, G. "A Universally Applicable Equation for the Instantaneous Heat Transfer Coefficient in the Internal Combustion Engine." SAE Technical Paper 670931, 1967.
24. Hohenberg, G. F. "Advanced Approaches for Heat Transfer Calculations." SAE International, 1979, doi:10.4271/790825.
25. Cho, S. "Study on the Effect of Cylinder Wall Temperatures on Knock Characteristics in Spark-Ignited Engine." Ph.D. Dissertation, Seoul National University, 2018.
26. Bonatesta, F., Waters, B., and Shayler, P. J., "Burn angles and form factors for Wiebe function fits to mass fraction burned curves of a spark ignition engine with variable valve timing." 11(2):177-86, 2010, doi:10.1243/14680874jer05009.

8. Glossary

0D: zero-dimensional

1D: one-dimensional

aBDC: after bottom dead center

aTDC: after top dead center

bBDC: before bottom dead center

CA: crank angle

CA0: crank angle at 0% mass fraction burned

CA90: crank angle at 90% mass fraction burned

CVVT: continuous variable valve timing

DoE: design of experiment

ECU: engine control unit

EGR: exhaust gas recirculation

EOC: end of combustion

EVO: exhaust valve opening

IGN: ignition

IVC: intake valve closing

LHV: low heating value

MAP: manifold absolute pressure

MAPO: maximum amplitude of pressure oscillation

MFB85: 85% mass fraction burned

N/A: natural aspirated

nIMEP: net indicated mean effective presusre

OF: overlap factor

PFI: port fuel injection

RGF: residual gas fraction

RMSE: root mean squared error

SI: spark-ignited

TVE: threshold value exceeded

WOT: wide open throttle